Summary of the Magnetic Confinement Theory and Modeling

Sergei Krasheninnikov

University California San Diego, USA

About 100 talks and posters have been presented by the authors from 30 countries

General impressions

1. Gyrokinetic modeling of core turbulence becomes routine. It boosts the understanding of complex nonlinear physics of core plasma turbulence, verified by analytic models and experimental data
2. Edge gyrokinetic codes are emerging and already produce interesting results

3 ELM modeling is progressing with both MHD and Braginskii codes

4. Theories of spontaneous core plasma rotation start to emerge
5. Integrations of the codes in global suites are in progress and in nearest future will help to analyze

Main sub-topics:

ELMs, pedestal + edge turbulence: 14

Fast ions: 7

Gyro-kinetic modeling and equations: 12

Heating and CD: 7

Integrated modeling (core & edge): 11

MHD + (from equilibrium to RWM to disruption mitigation): 24

Multi-scale turbulence (Drift waves + ZF + GAM +…): 14

“Others” (from dust to stochastic fields and to runaway electrons): 14

B. D. Scott, G. M. Staebler, D. R. Ernst, J. Candy, X. Garbet, Jiquan Li, P. D. Diamond, R. Singh, T. S Hahm, W. W. Lee, L. Chen, J. Connor, A. M. Dimits, A. Eriksson, Zhe Gao, K. Hallatschek, N. J. Joiner, Z. Lin, T. Matsumoto, V. S. Mikhailenko, N. Niyato, N. Nakajima, F. Ogando, X. M. Qiu, S. Satake, P. W. Terry, B. P. Van Milligen, M. O. Vlad, B. Coppi, K. C. Shaing, A. Ishizawa, A. J. Beculet, C. Bourdelle, T. M. Fulop, Jiaqi Dong, K. Gal, S. Hamaguchi, M. J. Hole, Y. Ishii, R. Ishizaki, P. J. Mc Carthy, P. Merkel, P. Rodrigues, O. Sauter, Abhijit Sen, F. S. Spineanu, Qingquan Yu, Linjin Zheng, V. A. Izzo, E. V. Belova, R. Farengo, V. V. Mirnov, R. Paccagnella, V. A. Svidzinski, H. L. Berk, F. Zonca, N. N. Gorelenkov, G. Pokol, K. Schoepf, G. Vlad, Z. T. Wang, Y. U. yakovlenko, V. Yavorskij, L. A. Berry, A. Cardinali, A. Fukuyama, R. W. Harvey, G. O, Ludwig, G. Park, C. S. Chang, A. V. Chankin, U. Deybelge, N. Kasuya, S. I. Krasheninnikov, A. A. Mavrin, N. Muzuguchi, J. R. Myra, V. Naulin, X. Q. Xu, R. Ball, R. H. Cohen,P. B. Snyder, H. R. Wilson, N. Hayashi. N. Aiba, G. T. A. Huysmans, S. E. Kruger, T. Onjun, V. Parail, H. R. Strauss, (J. D. Callen, D. Kh. Morozov, F. Porcelli, F. Jenko, C. Angeoni, G. Y. Fu, T. H. Watanabe)

ELMs, pedestal + edge turbulence

Edge turbulence:

Scott: turbulence shows a sharp change at LCFS from ITG inside to 2D interchange outside; global quasi-periodic bursts in both turbulence and transport at large source, relaxation of gradients

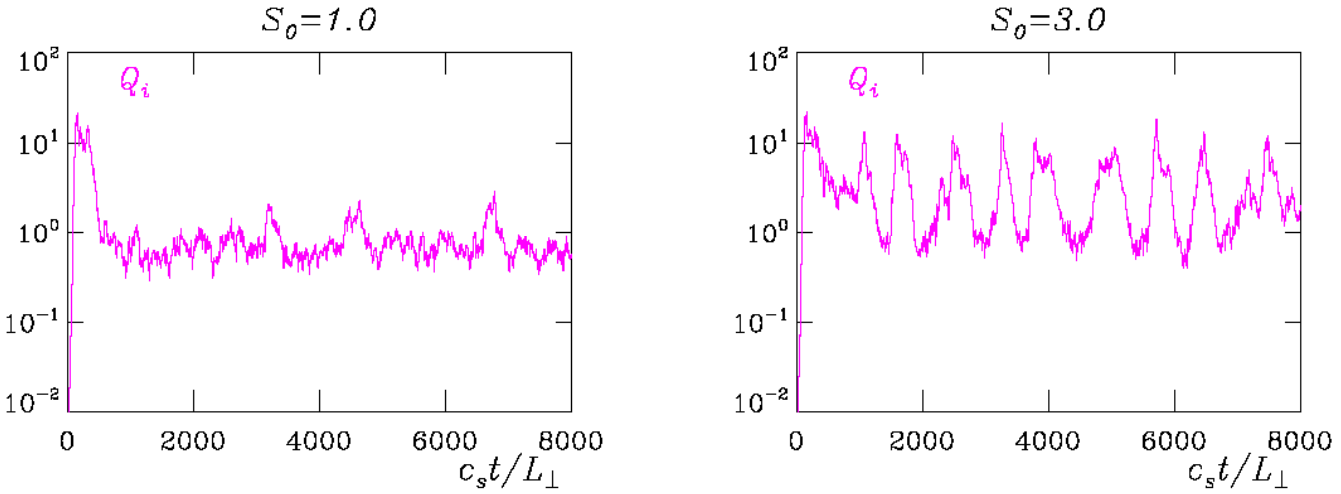

FIG. 1: Bursty turbulence for moderate edge turbulence (left) compared to global burst events (right) for larger heat source drive levels. The ion heat fluxes in terms of $p_i c_s(\rho_s/L_\perp)^2$ are plotted; the curves for the electron heat and particle fluxes are similar.

Naulin: 2D modeling of JET SOL turbulence with code ESEL; edge-SOL interface is the origin of intermittent bursts; blobs propagate into SOL; strong impact of collisionality; agreement with experimental data

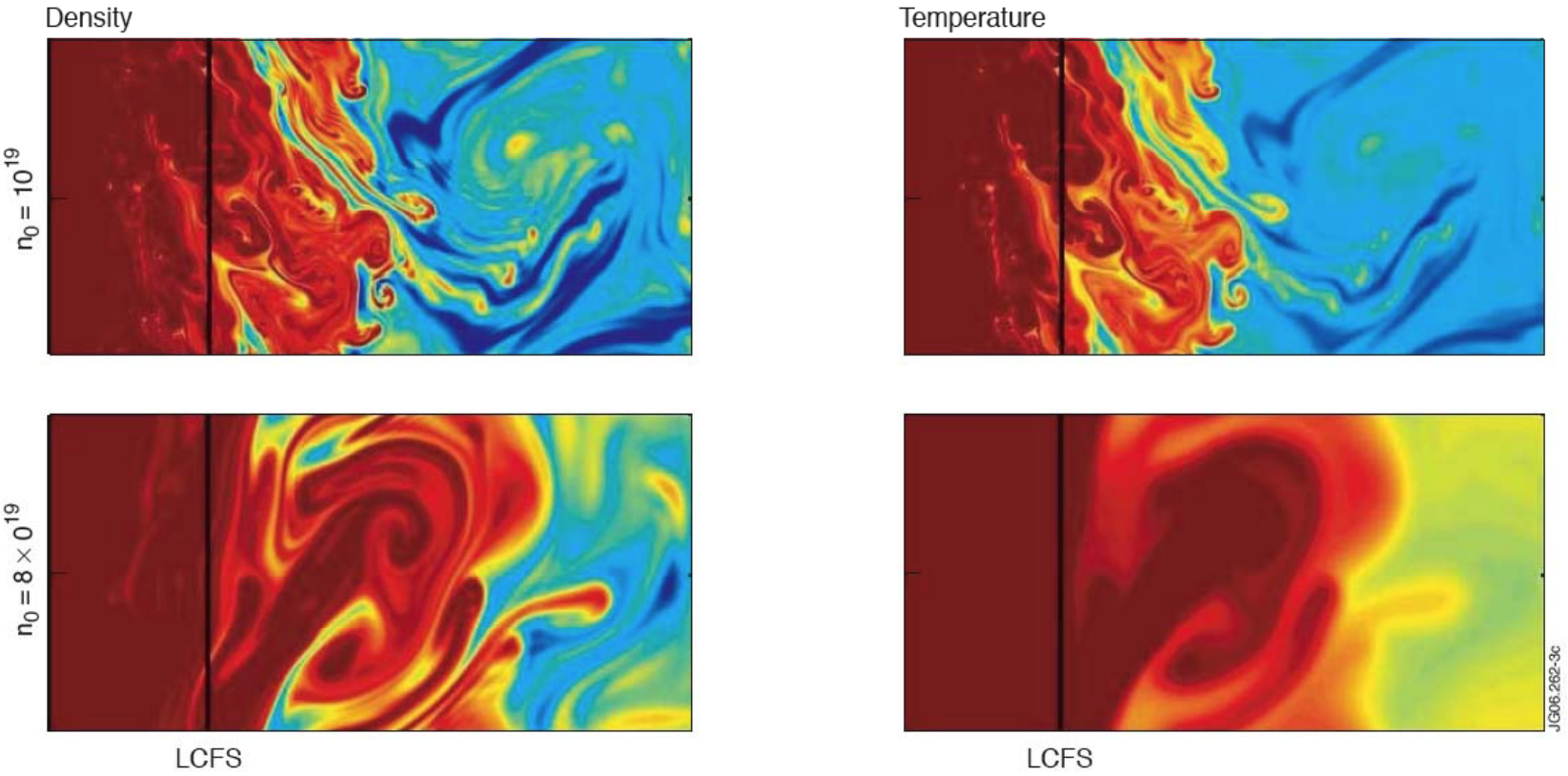

FIG. 3: Density and temperature fields for low and high collisionality.

Cohen: BOUT simulations of SN and UDN C-Mod plasma shows longer radial correlation lengths in UDN; curvature- and sheath-driven instabilities can exist in the private- as well as common-flux regions of divertor legs, isolated from the main SOL by X-point

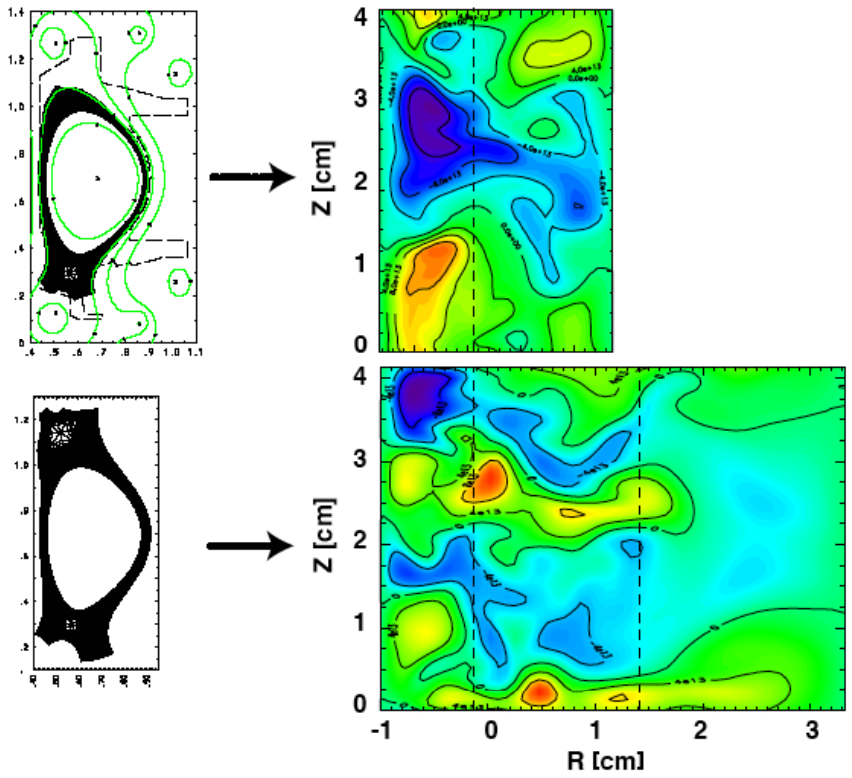

FIG. 1: Fluctuations of density at outer midplane for single-null and double-null BOUT runs

Divertor/Private region turbulence, driven by inclined divertor plate, might be consistent with recent MAST experiments data!

Myra: theoretical prediction of blob dynamics is in a reasonable agreement with experimental data ($V_* = C_s\left(L_\parallel^2 \rho_s^4 / R^6\right)^{1/5}$); transport of angular momentum with blobs can explain spontaneous plasma rotation phenomena seen in experiments

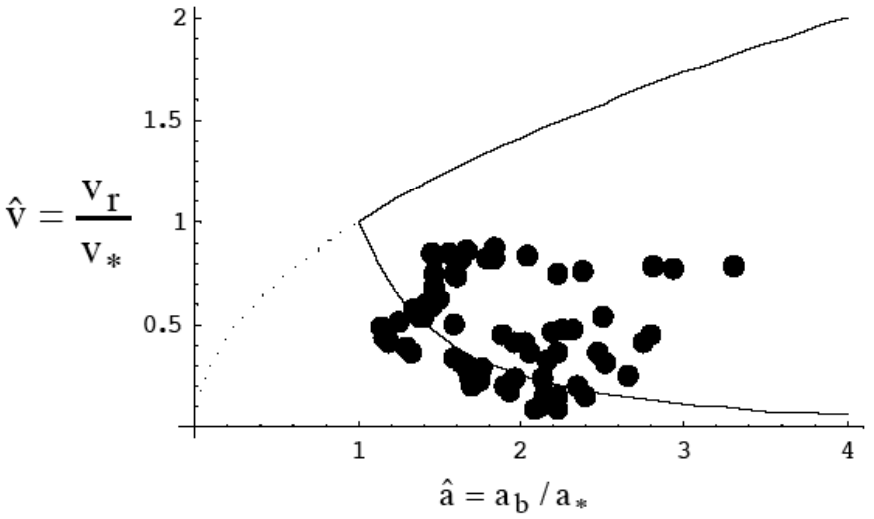

FIG. 3. Observed radial blob velocities (filled circles) in dimensionless parameter space of velocity and blob scale size. The data is approximately bounded by a theoretically predicted minimum and maximum (solid lines).

ELMs:

Huysmans: first application of newly developed nonlinear MHD code JOREK capable to deal with X-point geometry;

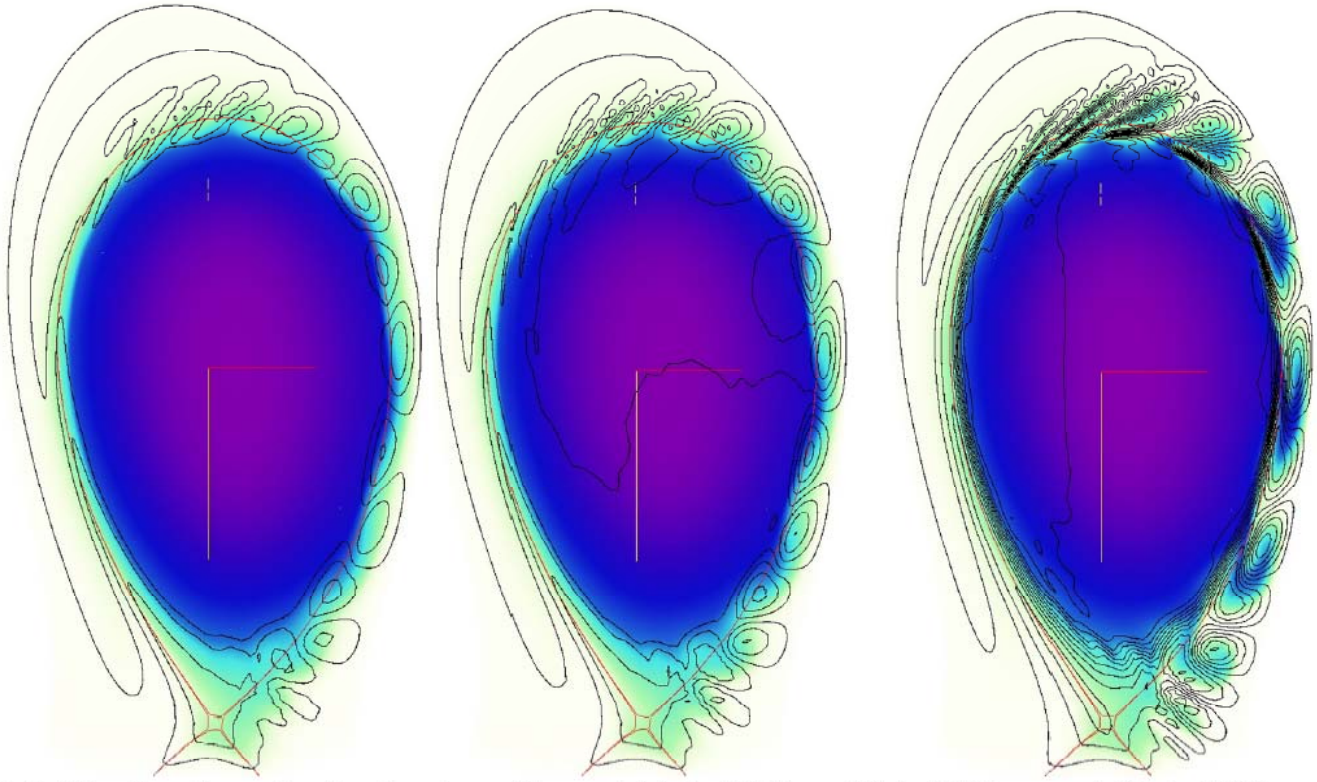

FIG. 6. The density and velocity streamlines at (a) t=2650 τ_A, (b) t=2700 τ_A and (c) t=2890 τ_A due to an n=6 ballooning mode.

Wilson: The final state of the plasma edge plasma profile after bursts of peeling modes is deduced by an extension of Taylor relaxation theory; theory gives $\Delta W_{ELM}/W_{PED}$ ~ few percent; these predictions are consistent with measurements from Type III ELMs, for which the theory is thought to be most relevant

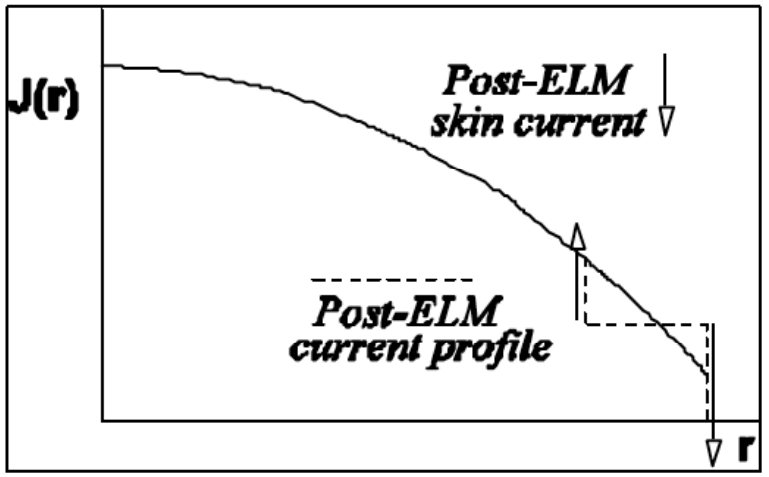

Figure 1: A schematic of the pre- (full) and post-ELM (dashed) relaxed current profiles showing the formation of skin currents

Mizuguchi: nonlinear MHD simulation reproduces several characteristic features of type-I ELM in ST including: intermediate-*n* precursors, low-*n* structure on the crash, and the formation and separation of the filament (a); for the peeling mode case (type-III ELM ?!), no prominent filament structure is formed (b) in contrast to the ballooning case

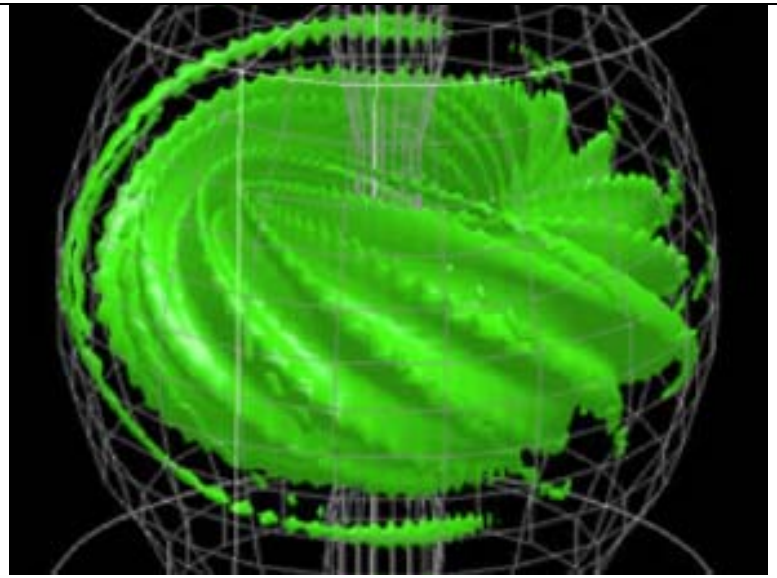

(a)

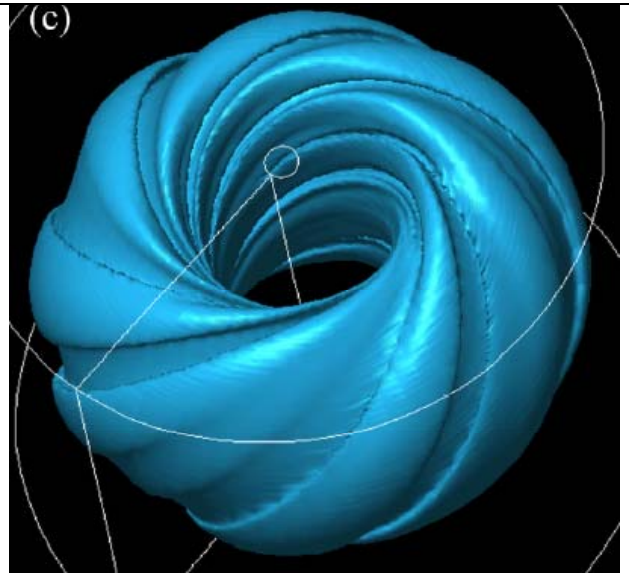

(b)

Snyder: QH-mode operation may correspond to pedestal particle/energy drain by saturated low- n kink/peeling mode destabilized by high bootstrap current and rotation; RMP just substitute low- n kink/peeling mode; nonlinear ELM simulation with BOUT shows filament formation

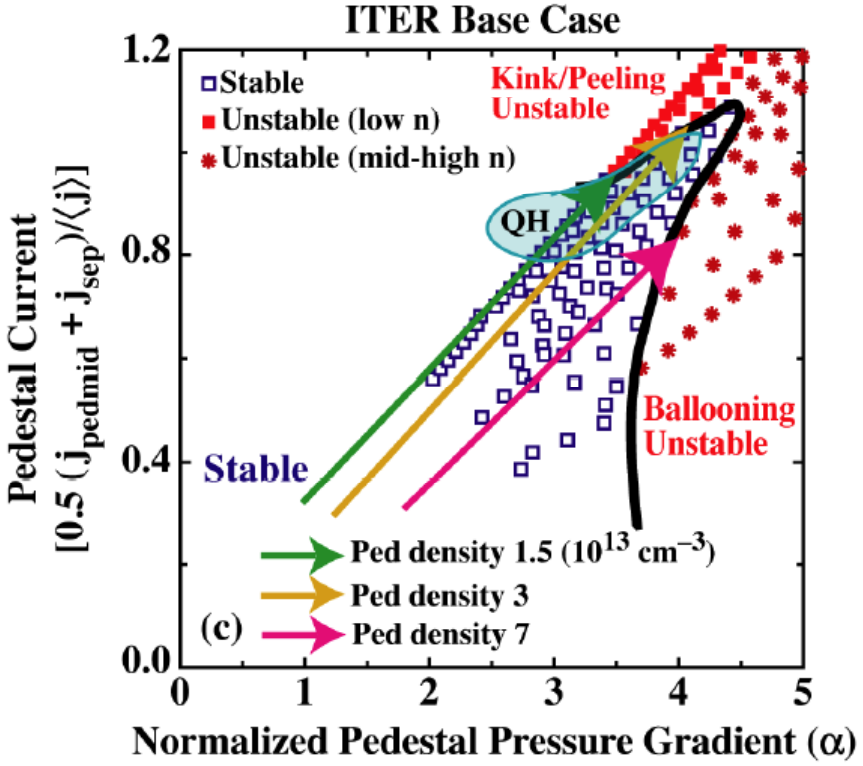

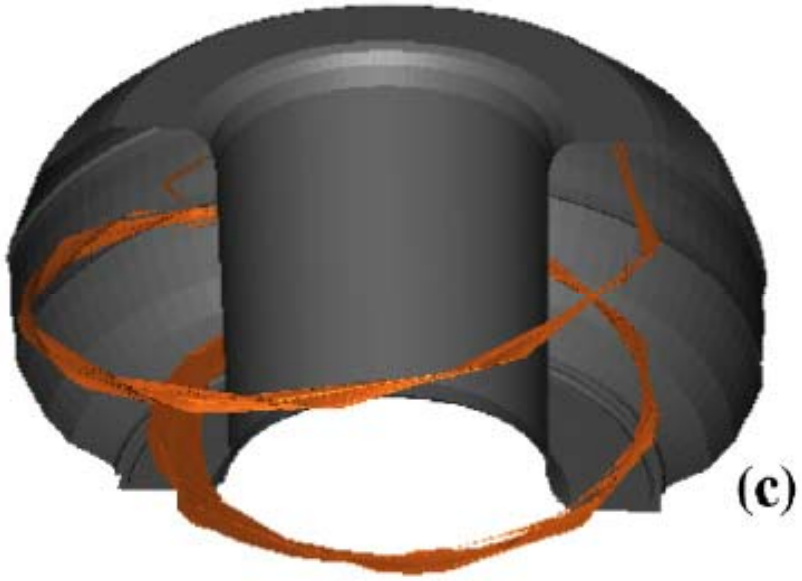

Filament of plasma propagates rapidly toward the wall

Kruger: ELM modeling for DIII-D case with NIMROD

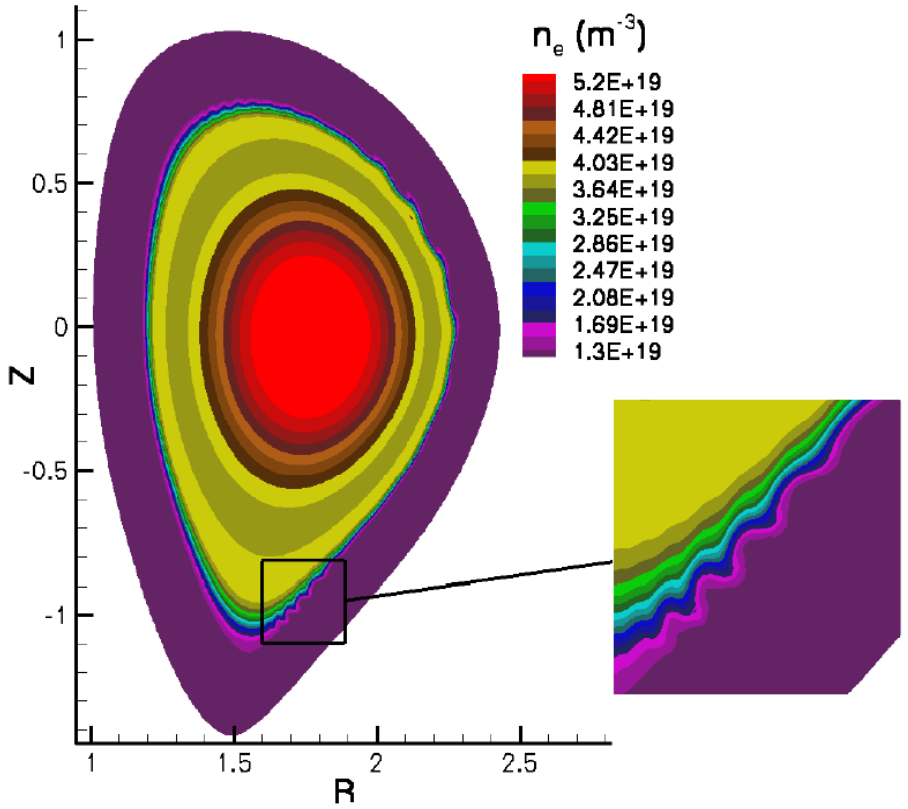

FIG 8. Number density at toroidal angle ϕ=0 at 7.92 μs into the nonlinear two-fluid computation.

Strauss: DIII-D and ITER ELM modeling with M3D code

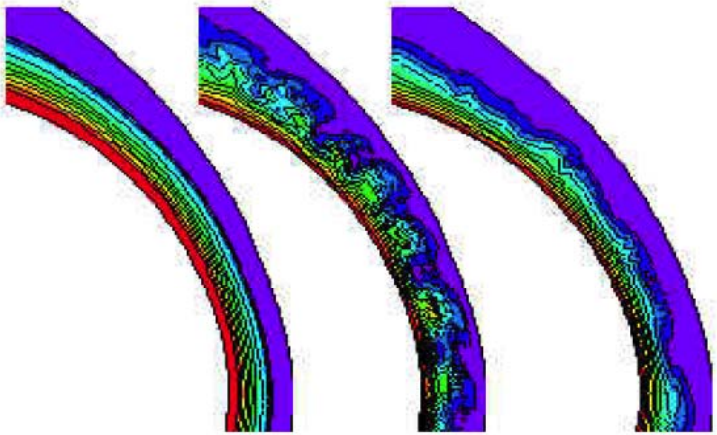

Figure 1. pressure at (left to right) times t=27 t_A, t=67 t_A, and t= 106 t_A in a DIII-D ELM simulation.

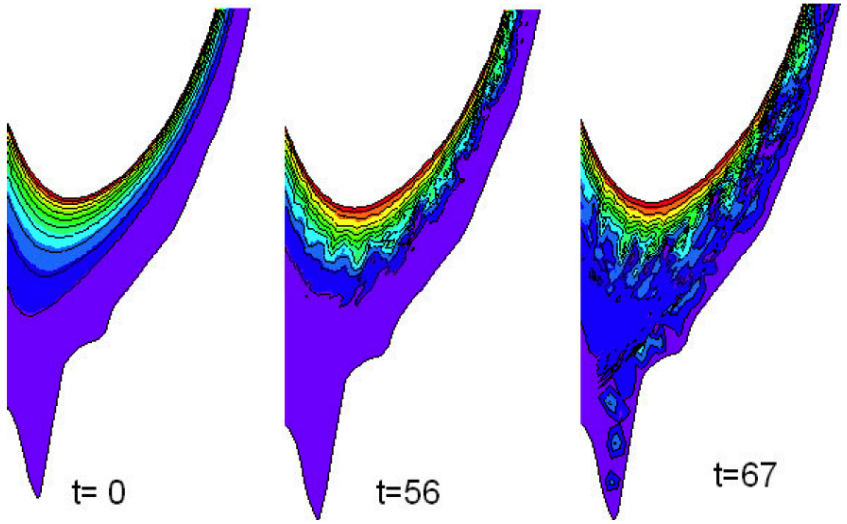

Figure 2. ELM simulation in ITER geometry. Note outflow to divertor at t =67 t_A.

Parail: both magnetic ripple and RMP have good potential for use as a tool for ELM mitigation; Since magnetic ripple increases ion transport and RMP electron transport, a combination of these two methods might give a very versatile tool to control both electron and ion transport in the pedestal region of the plasma.

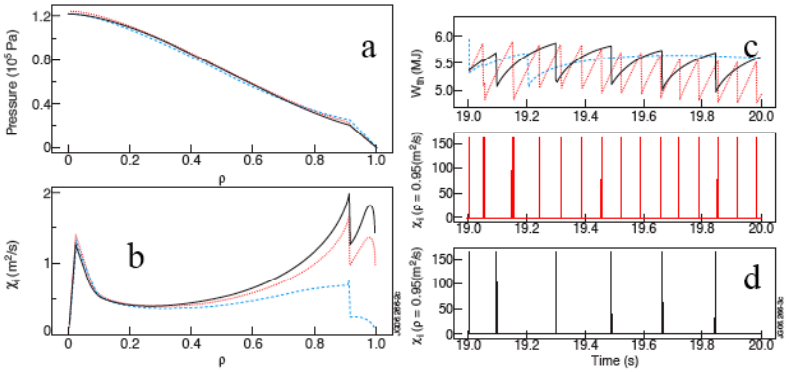

FIG. 3. Predictive transport modelling of JET plasma with the different level of wide ripple transport: red- without ripple, blue- medium ripple, pink– maximum ripple. a) plasma pressure just before ELM; b) ion thermal conductivity before ELM; c) time evolution of the energy content; d) ELM frequency for three level of convective losses.

Gyro-kinetic modeling and equations

Garbet: semi-Lagrangian scheme is used in upgrated 5D GYSELA full-f code, which is used for toroidal ITG turbulence modeling; impact of initial f may be crucial: non-canonical f results in the development of large flows, which suppress turbulence

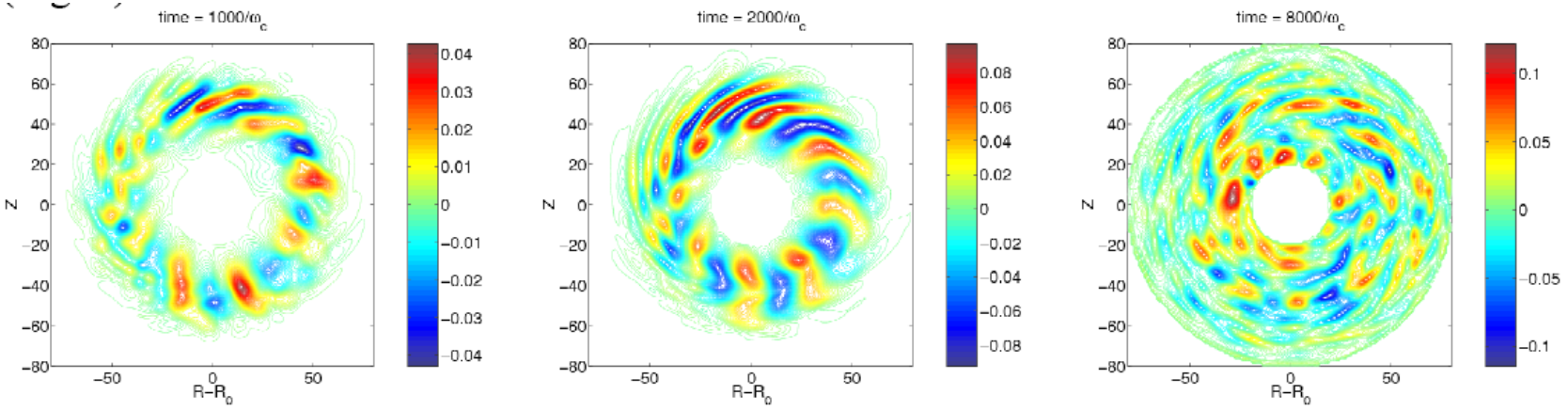

Fig.6: Contour lines of the fluctuations of electric potential $e(\phi-\phi_{eq})/T_{eq}$ for ITG turbulence with zonal flows when the initial distribution function is canonical.

Candy: GYRO modeling of coupled ITG/TEM-ETG turbulence; back-reaction of ETG on ITG is negligible (agrees with Holland/Diamond theory); ETG turbulence suppression is due to ITG modulation of the T_e gradient; gyrokinetic ions are important for ETG saturation; contribution of ETG in heat conduction is ~ 5% unless ITG is suppressed

Connor: GS2 modeling of ETG in MAST gives heat conduction ~5 m^2/s, which is much larger mixing length estimates due to large streamers

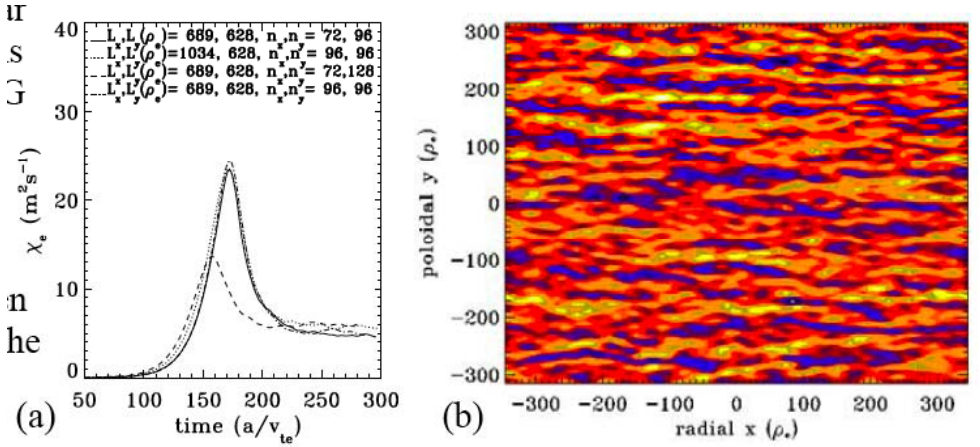

Figure 7: Nonlinear ETG simulations for MAST #6252 at ψ_n= 0.4. (a) Electron thermal diffusivity as a function of time for various flux-tube resolutions. (b) Contour plot of electrostatic potential in the x y plane at the intersection of the flux-tube with the outboard equatorial mid-plane.

Xu: gyrocode for the edge (4D TEMPEST: GAM collisionless dumping results in RH residual; 5D is in progress)

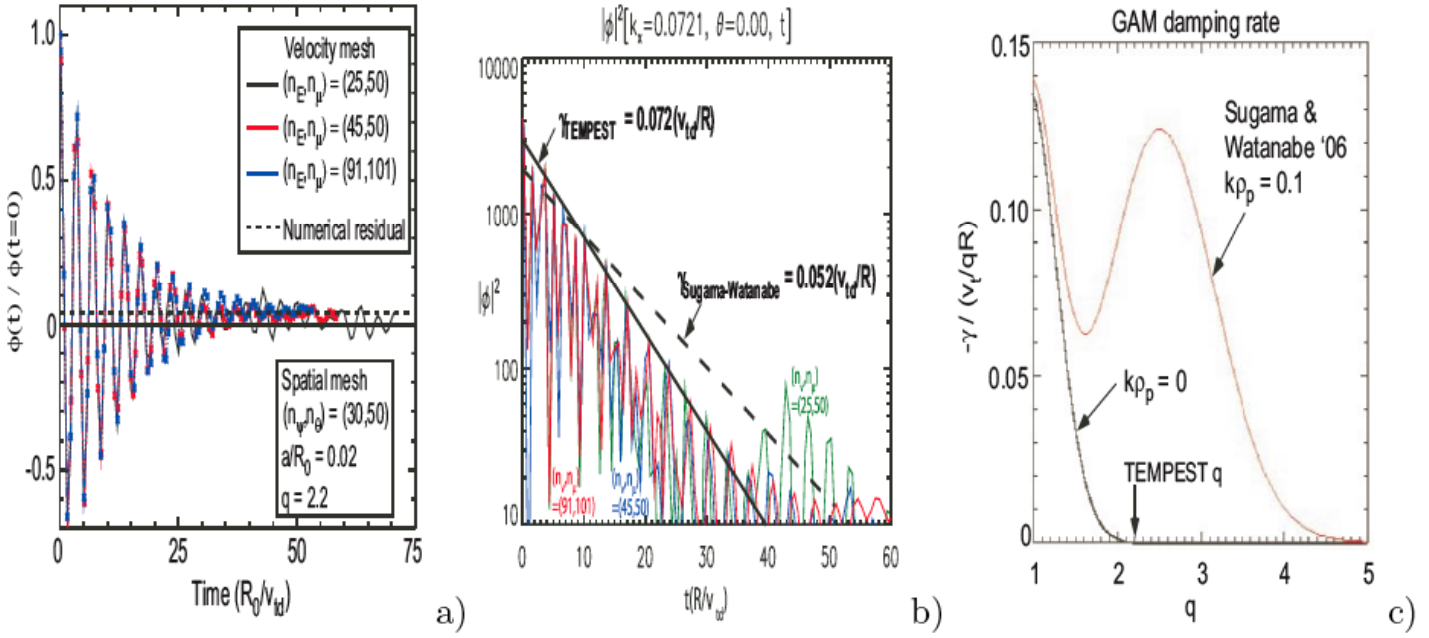

FIG. 3: (a) Time evolution of the zonal-GAM potential shows GAM oscillation, collisionless damping, and residual for a large-aspect-ratio circular geometry with $q = 2.2$ and $\epsilon = 0.02$ with three different velocity resolutions; (b) Comparison of simulation results with theory for GAM damping rate with three different velocity resolutions in finite banana orbit regime; (c) GAM damping rate vs q with finite banana orbit effect (yellow) and without finite banana orbit effect (black) from Sugama and Watanabe theory [14].

Watanabe: modeling of GAM in helical systems with gyrokinetic-Vlasov (GKV) agrees with theory; ITG stability and turbulence reported

Hahm: modeling of ITG spreading with GTC code; spreading occurs in nonlinear regime

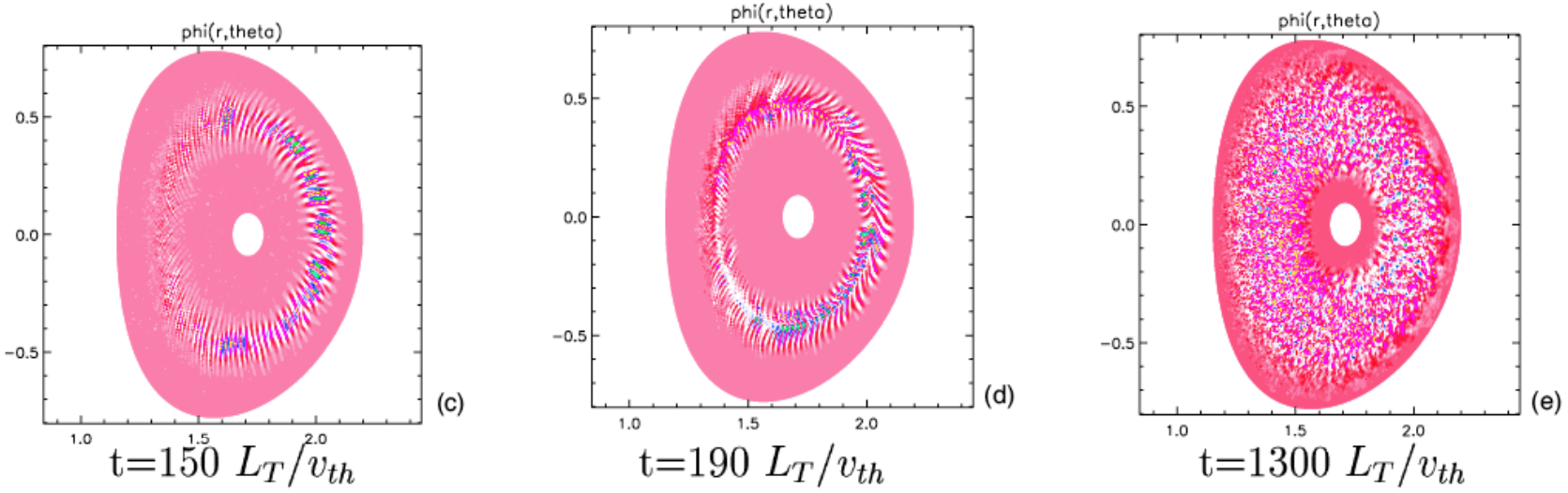

Jenko: GENE – fully e and i gyrokinetics, finite beta, full e and i collisions, beam ion species, general geometry and ExB shear; new analytic QL expression for TEM turbulence captures very well the physics of TEM fluxes

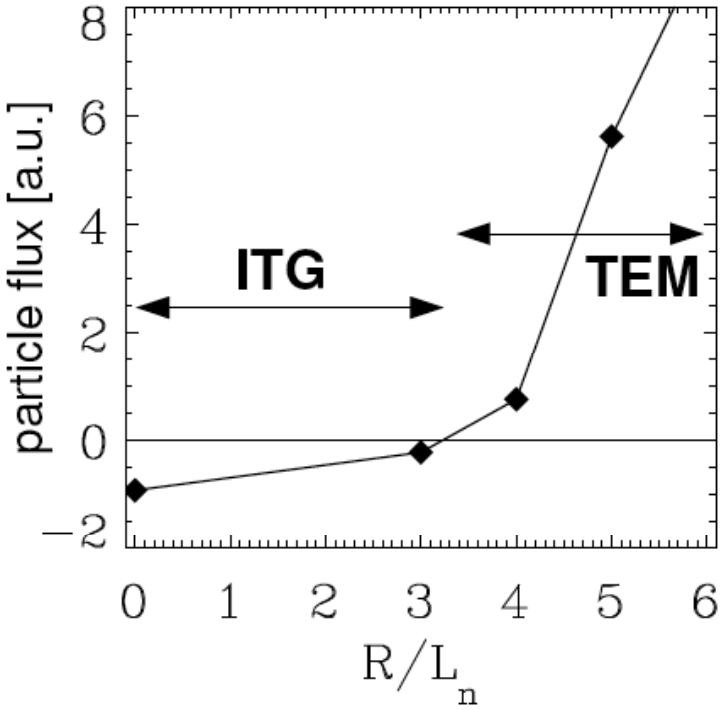

Ogando: development of full f gyrokinetic code ELMFIRE

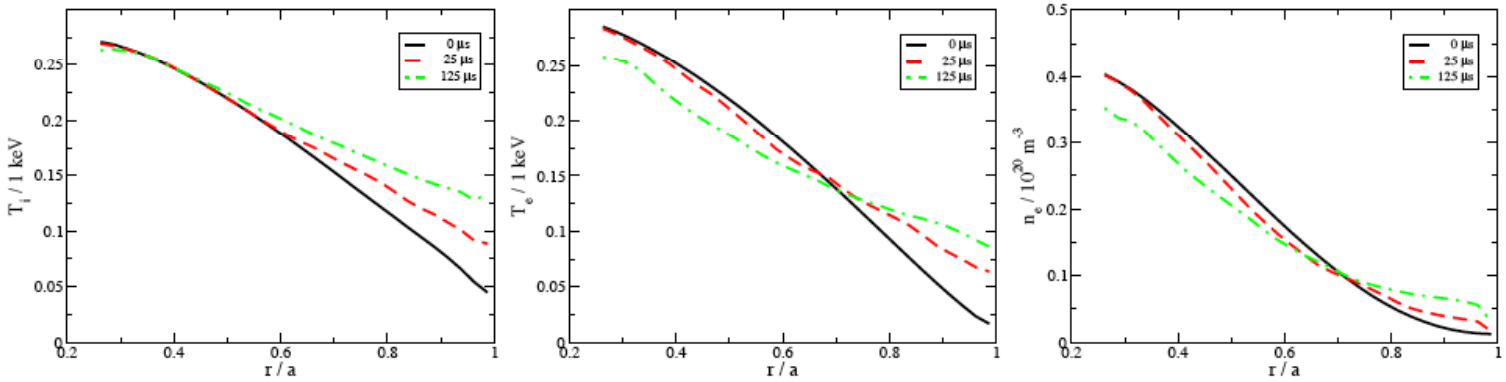

Figure 2: Radial temperature profiles for electrons (T_e) and ions (T_e), and density profile for electrons at simulation times of 0 μs, 25 μs, and 125 μs. Initial temperature for ions and electrons are the same.

Ernst: modeling of TEM in C-Mod with GS2 code and comparison with experimental data (Phase Contrast Imaging); good agreement is found

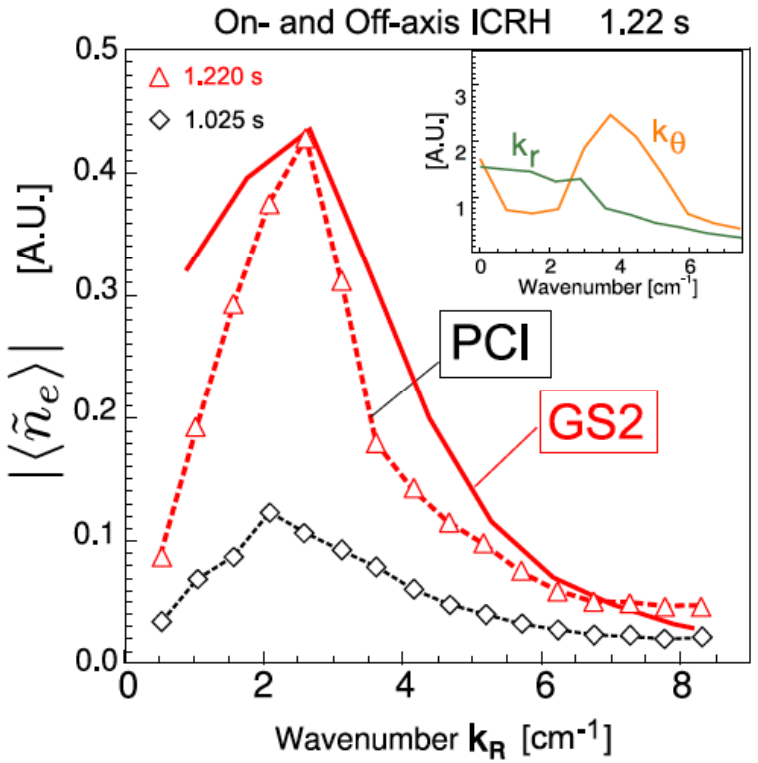

FIG. 7. Comparison of spectra of density fluctuations from PCI, and from GS2 nonlinear simulation with synthetic PCI diagnostic. GS2 spectrum is linear combination of radial and poloidal wavenumber spectra shown in inset.

Dimits: ETG and ITG modeling with PG3EQ

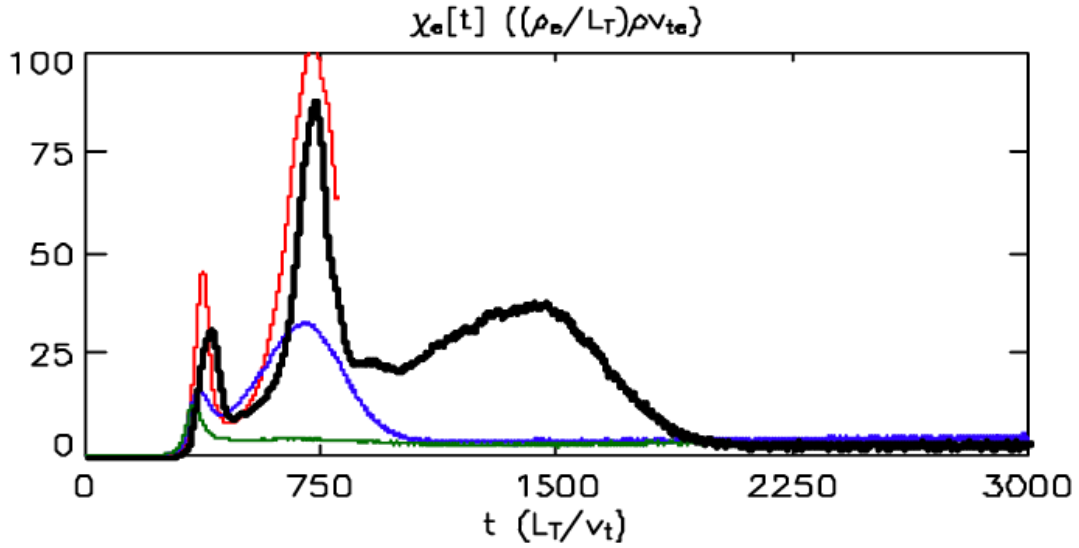

FIG. 1. χ_e vs. time from a particle-number and flux tube cross-section convergence study of ETG turbulence (with r/R_0=0.18), including runs in a flux-tube with cross-section $500\rho_e \times 125\rho_e$ with 2 particles/grid cell (green curve), 4 particles/grid cell (blue curve), and 16 particles/grid cell (red curve); and a flux-tube cross-section of $250\rho_e \times 62.5\rho_e$ with 16 particles/grid cell (black curve).

Lee: ITG and ZF modeling with PIC code GTC

Fast ions (7)

Berk: frequency sweeping of global GAM caused by off-axis ICRF heating (explains JET and NSTX experiments)

5. n=0 chirping in JET

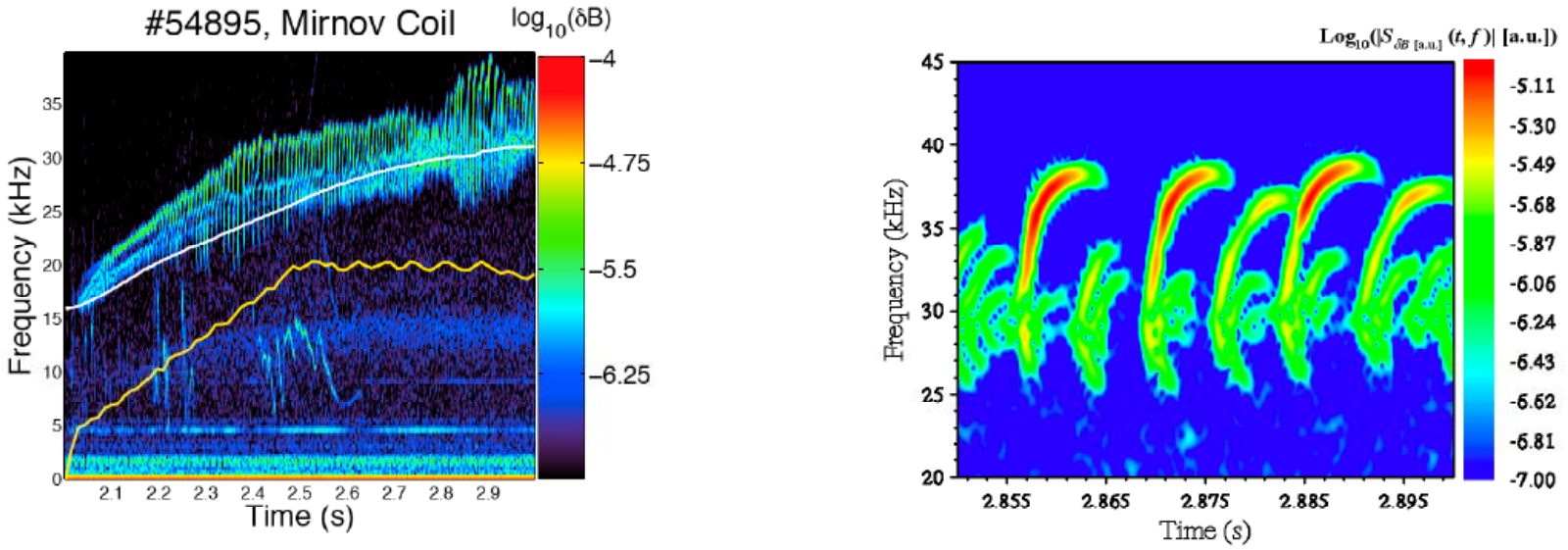

FIG. 3(a) Sustained chirping of the n=0 (GAM) that emerges after the onset of off-axis ICRF power (brown curve) with the onset frequency proportional to $T_e^{1/2}$ *(white curve). (b) Zoom of the frequency chirp signal. The upward (downward) sweep can be attributed to the formation of clumps (holes) due to an effective negative mass effect in mirror trapped particles(ref.).*

Gorelenkov: Compressional Alfven Eigenmodes (CAE) driven by phase space gradient is measured in NSTX and DIII-D and analyzed numerically in a first time with code NOVA. Might channel energy from fast ions (including alphas) to heat thermal ions

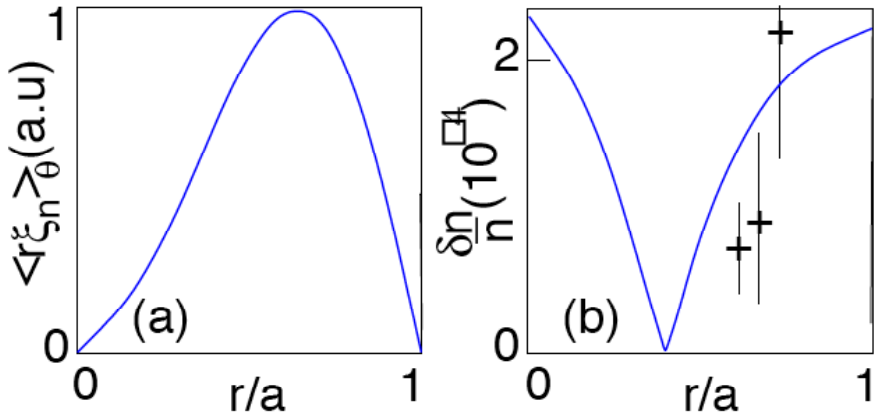

FIG. 7: $(3/2, 1/2, 0)$ CAE plasma displacement (a) in the midplane on the LFS in NSTX. (b) Shows density perturbation in the midplane. Points marked with plus signs correspond to experimental data from the reflectometer diagnostic. Shown also are the error bars for each point.

Yakovenko: energetic ion redistribution during sawtooth crash in NSTX, the code GYROXY has been extended to include a model of the EM field evolution during a Kadomtsev-type sawtooth crash; the model, in particular, can take account of the diamagnetic perturbation of *B* due to the pressure redistribution

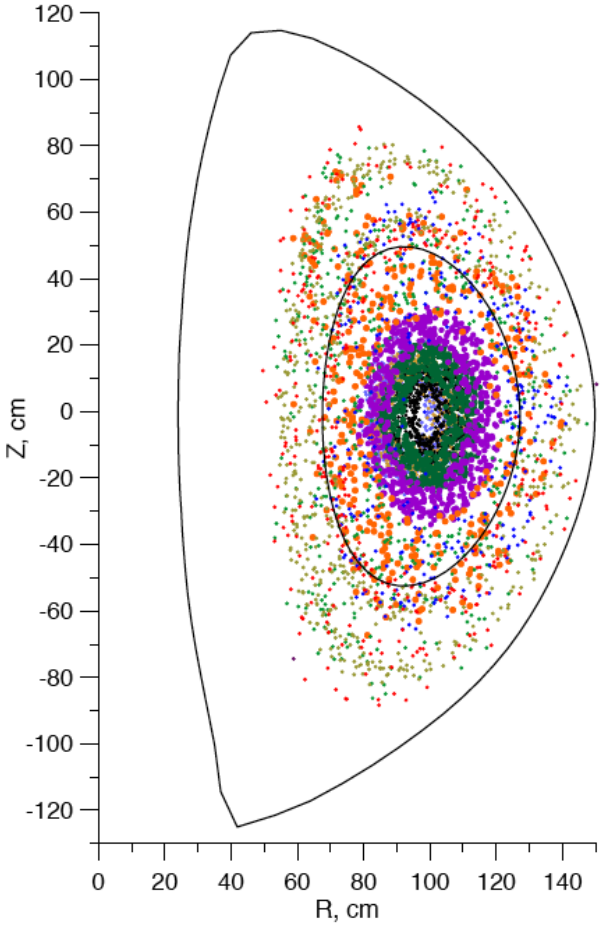

Yavorskij: Evolution of Fusion-born alphas in JET tritium NBI blips

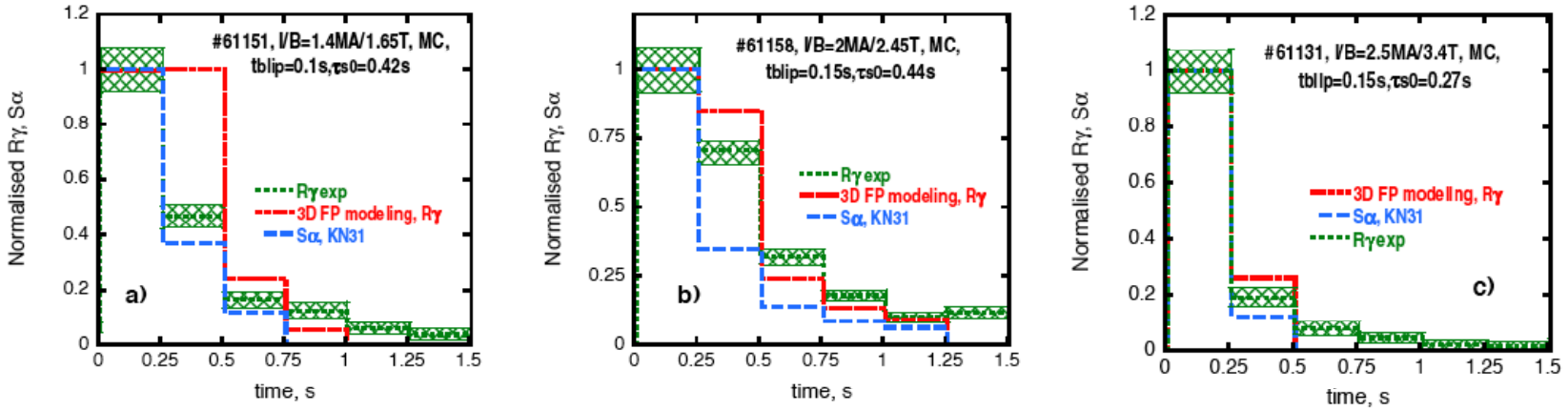

Fig. 13 Measured and modelled rates of gamma and neutron emission in the cases of plasmas with low current (figure a, b) and in those with sawtooth activity (figure c)

Heating and CD

Park: 6D test particle code in realistic tokamak geometry models ion interaction (full Lorentz force) with given electromagnetic field to verify quasilinear ICRH operator, reduced 5-1/2D method is proposed

Fukuyama: ICRF self consistent full wave analysis with the modification of ion distribution function with code TASK

Harvey: EBW studies – emission and absorption and current drive with non-Maxwellian distribution, The efficiency of EBWCD for NSTC ~45 kA/MW

Berry: ICRF on ITER with AORSA and TORIC (full wave simulation codes) Coupled to CQL3D FP code

Integrated modeling (core & edge)

Becoulet: “Fusion Simulator” – equilibrium and linear MHD stability + nonlinear MHD and disruption + transport and discharge evolution + transport and micro-stability + heating and CD & 2 support projects (code platform and data coordination)

Staebler: a new theory based transport model (trapped-gyroLandau-fluid, TGLF) has been developed; it accounts for ITG, TEM, and ETG; quasilinear expressions with mode saturation from GYRO are used; no experiment based fitting parameter

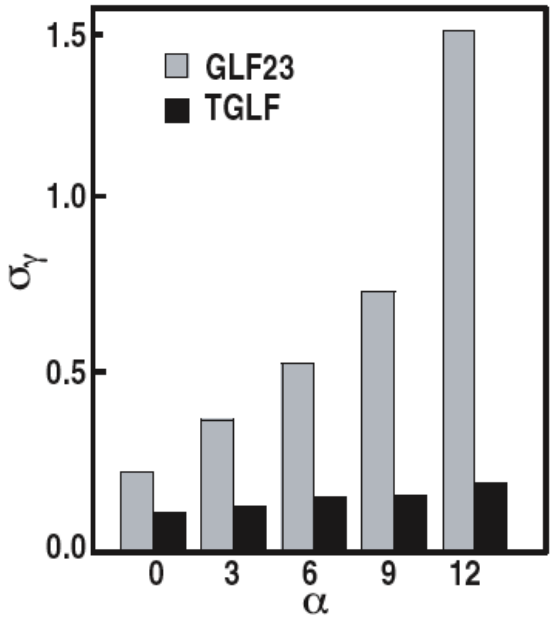

Chankin: in both Ohmic and H-mode shots SOLPS shows lower temperature and higher density in divertor in discrepancy with experimental results; nonmaxwellian features (!?)

Porcelli: integrated modeling of sawtooth oscillations on TCV and JET; includes MHD, fast ions and superthermal electron dynamics

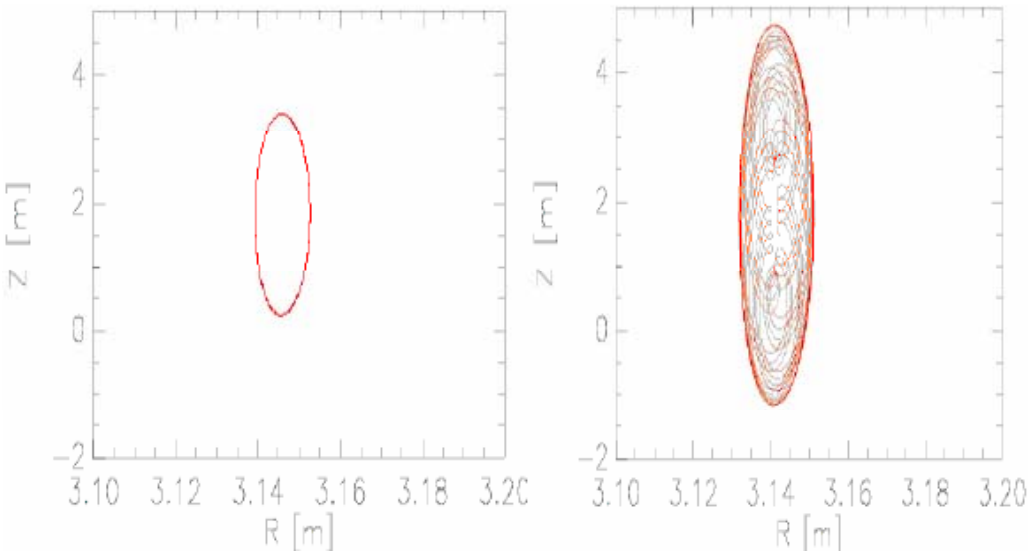

Pacher/Dies: DEMO(-s) modeling with ICPS (Integrated Core Pedestal SOL) and CRONOS; ~3GW of power with Q>50 and P_{div}~10mW/m^2

Hayashi: ELM energy loss by pedestal MHD and SOL transport

C. S. Chang: edge integrated gyrokinetic simulator

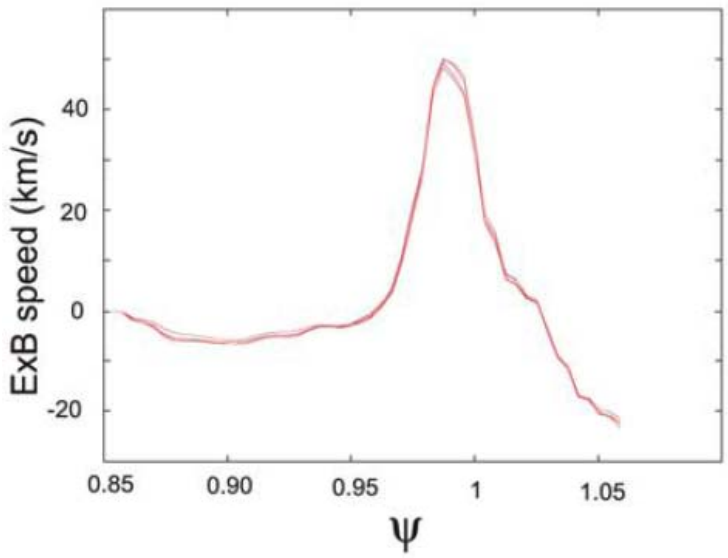

Fig. 6. Strongly sheared ExB poloidal rotation

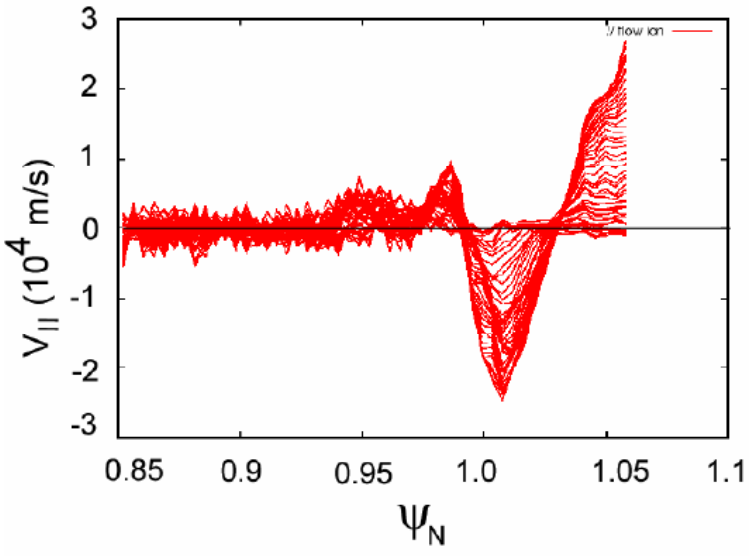

Fig. 8. Sheared parallel rotation in an H-mode-like DIII-D plasma geometry

Nonmaxwellian features are important and cannot be captured in standard neoclassical theory; neoclassical flow shearing is strong enough to suppress turbulence

MHD + (from equilibrium to RWM to disruption mitigation)

Maget: interplay of LHCD with MHD activity; MHD simulations with 3D MHD code XTOR

Reiman: breaking of flux surfaces at high (~3%) in W7AS calculated by 3D PIES equilibrium code; flux surfaces start to broke at outer side due to compression of Ψ due to Shafranov shift; stochastic region decreases with decreasing β going to zero at β <1%.

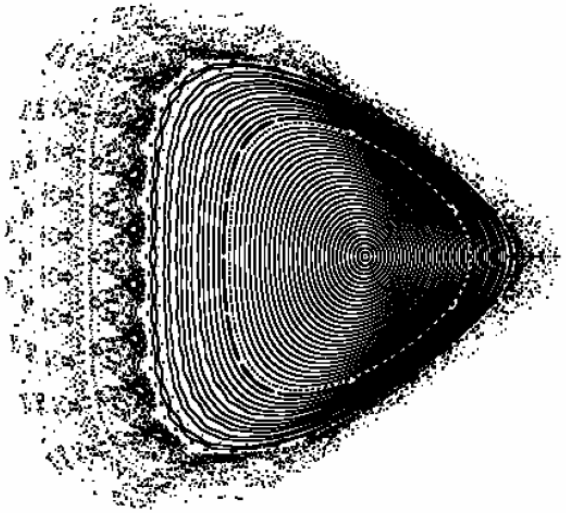

FIG. 1. *Poincare plot calculated by PIES for a β = 2.7% W7AS plasma.*

Izzo: NIMROD simulation of disruption mitigation by high pressure gas injection into Alcator C-Mod; 2/1 (stochastization) and 1/1 (collapse of central T) modes are the most important players

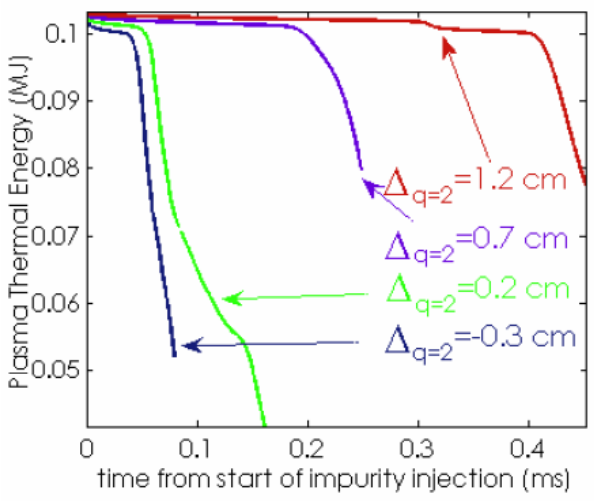

Ishizaki: MHD simulation of ablation cloud with 3D MHD code CAP; drifting motion of plasmoid into low B region; increase of front density gradient; pressure oscillation due to fast compressional Alfven wave

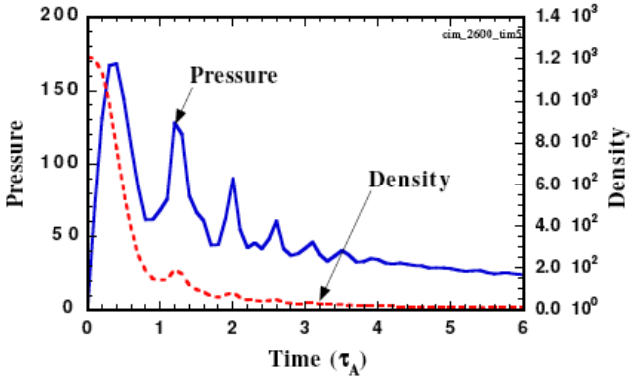

Rodrigues: solution of GS equilibrium with current hole in JT-60 and comparison with experimental data

Sen: modification of magnetic islands by the shear flow; Δ' modification and a generalized Rutherford model equation incorporating modified Δ' and inner layer dynamics is derived

Sauter: stabilization and control of NTM in burning plasmas with ECCD

Mirnov: two fluid dynamos and edge-resonant m=0 tearing instability in RFP

Dong: MHD flow layer formation in the vicinity of rational q may explain the ITB formation

Zonca: theory and experimental evidence of electron fishbones; modes are driven by barely trapped supra-thermal electrons with inverted spatial gradient formed due to ECRH (DIII-D) and LH (Compass-D); electron fishbones with small ρ_e in current tokamaks can simulate ion fishbones with small ρ_i in ITER

Multi-scale turbulence (DW+ ZF + GAM +…)

Miyato: global ITG simulation shows nonlocal behavior of GAM caused by coupling to the turbulence

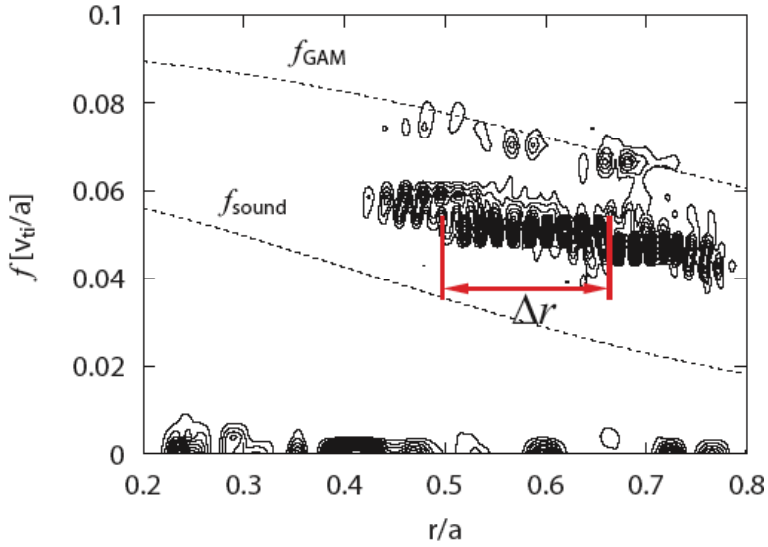

L. Chen: nonlinear evolution equation derived in the paper is used to get nonlinear equilibria generated by DW- ZF interactions

Diamond: Vortex Mode (low m) is generated by inverse cascade in the vicinity of low q resonances works as an effective ZF and can explain ITB formation

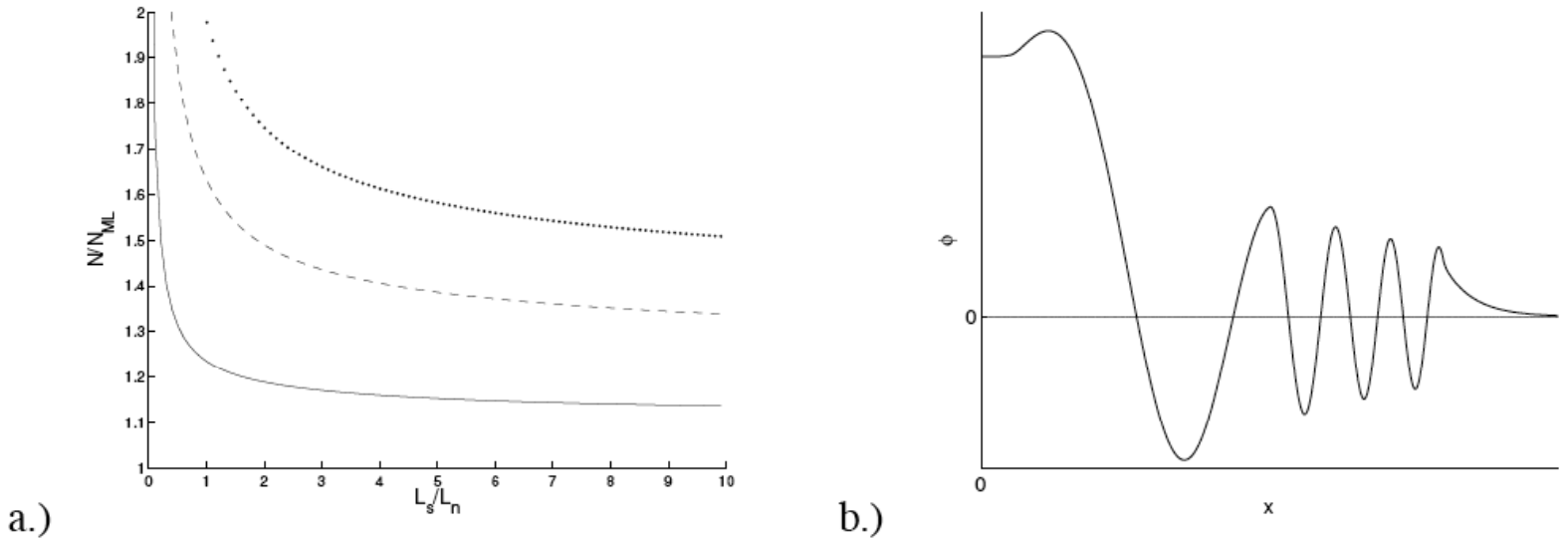

Figure 2: a.) Saturated intensity of drift wave turbulence for three values of viscosity for the parameters $\gamma_d/\gamma_k = 1$, $\eta/D_{GB} = 1/10$, $\beta = 1/20$, $m = 2$, and $\rho^* = .01$. The solid curve corresponds to $\nu_c/D_{GB} = .01$, the broken curve to $\nu_c/D_{GB} = .05$, and the last curve to $\nu_c/D_{GB} = .1$. b.) Sketch of radial potential profile of the vortex cell.

Hallatchek: magnetic shear, q, and geometry affect GAM and, therefore, transport; e.g. elongation reduces GAM frequency and increases energy transfer into GAM-> reduces heat flux

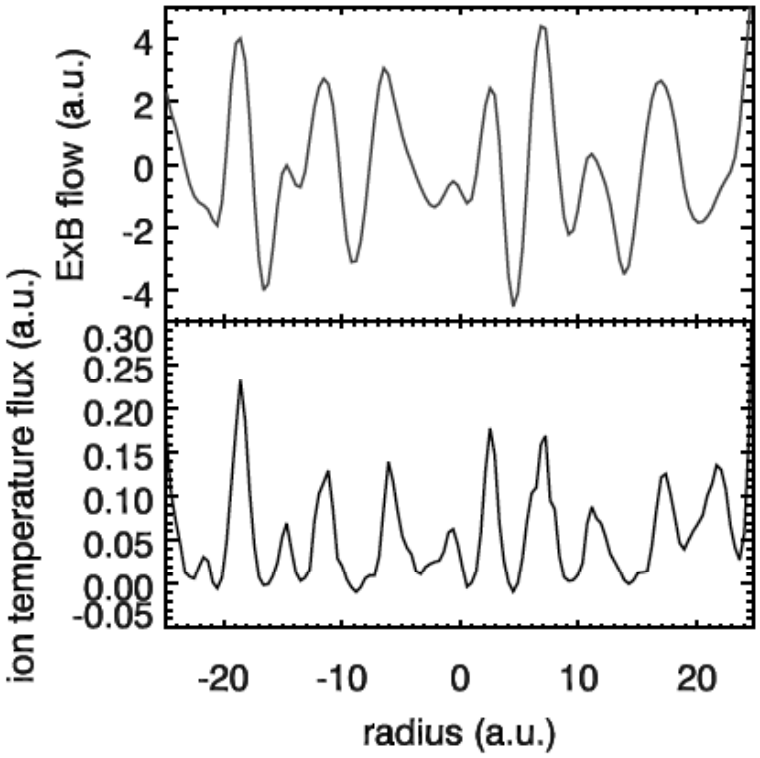

κ=2

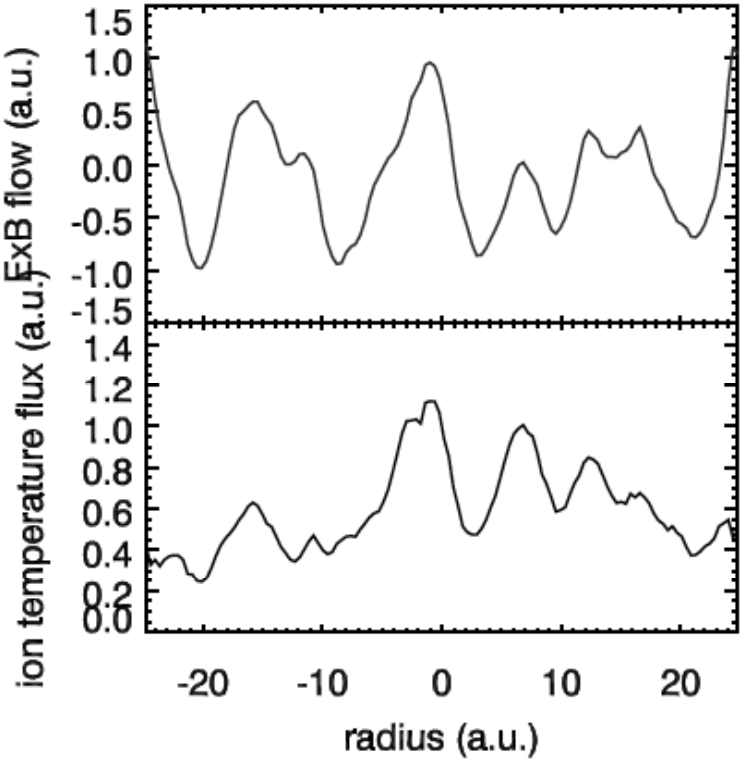

κ=0.5

Ishizawa: 3D two-fluid simulation of the interactions of micro-turbulence, tearing mode, and ZF.

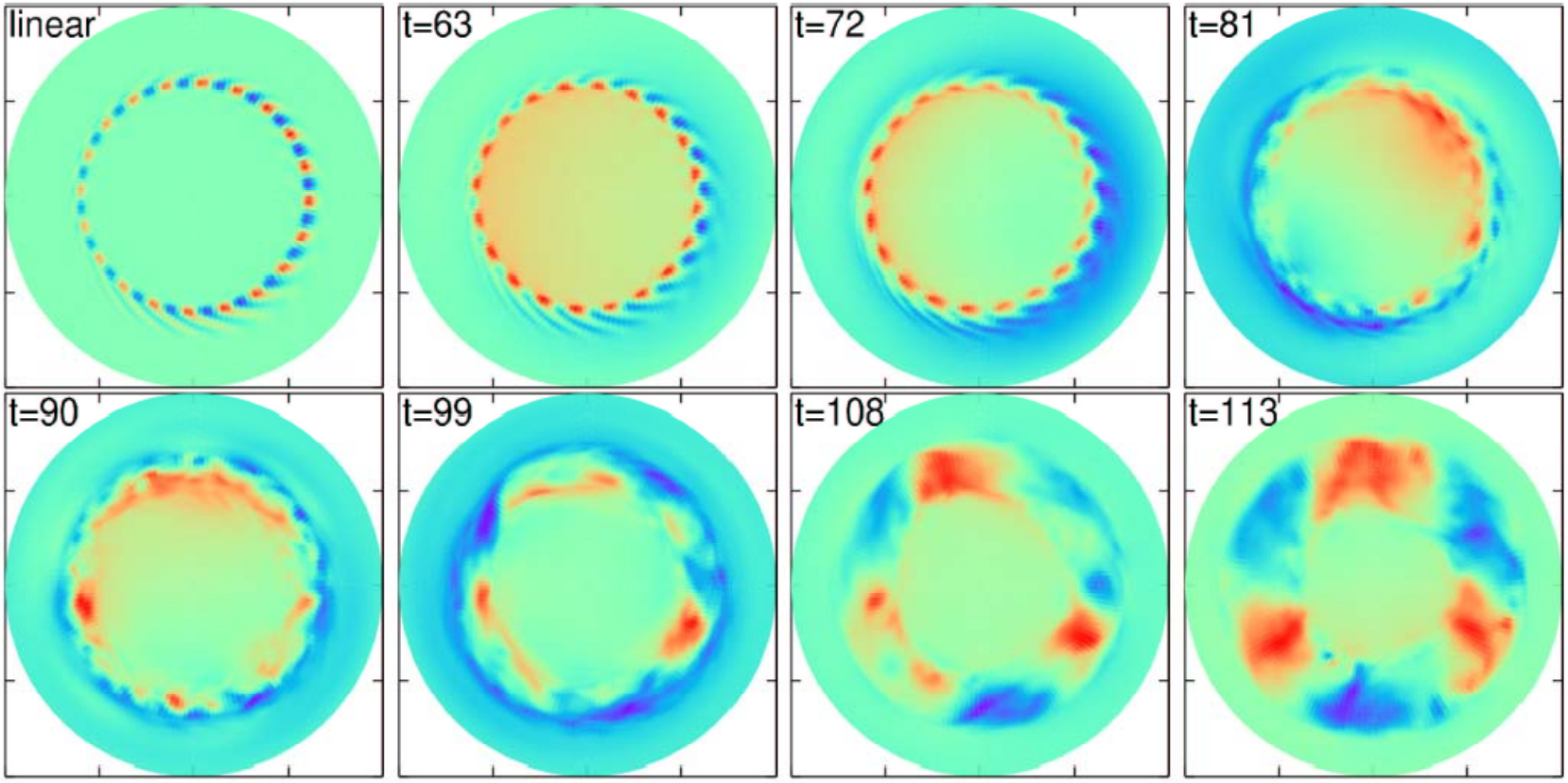

Coppi: “Neo-Drift-Tearing” mode is found; can produce significant magnetic islands in the presence of electron temperature gradients due to enhanced cross-field electron heat transport in stochastic microscopic B-field

Terry: inward particle flux in TEM turbulence – linearly stable mode is excited nonlinearly, saturated due to ZF, and gives large inward pinch which is missed in quasi-linear theory

Li Jiquan: 3D gyrofluid and gyrokinetic modeling of an impact of ZF on ITG and ETG turbulence; ZF changes the radial power spectrum from Kolmogorov-like power-law to exponential one

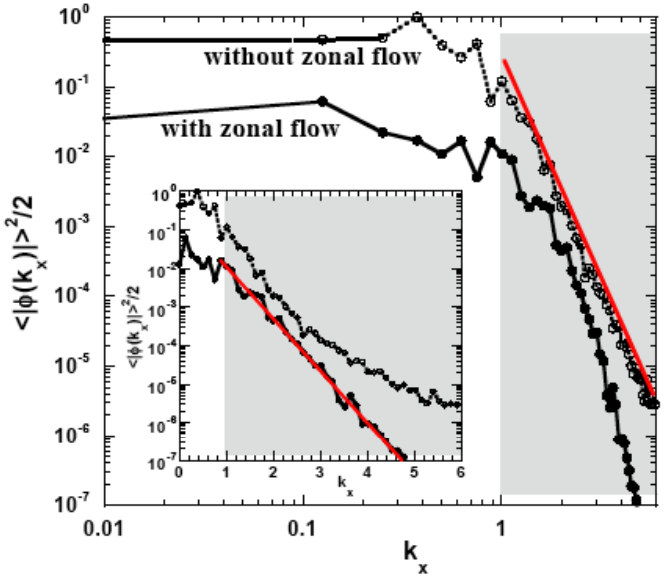

Gao Zhe: eigenmode analysis of GAM and zonal flows are performed for collisionless plasma and a new low frequency branch is found ($\tau=T_e/T_i$)

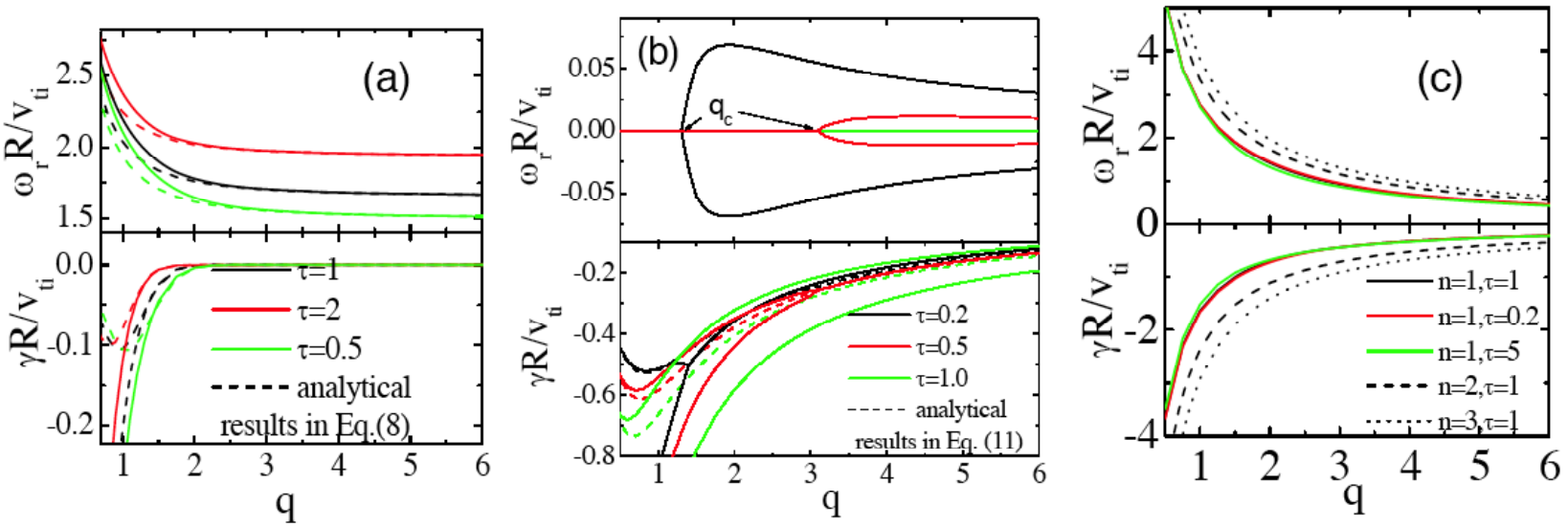

Fig.1. The frequency and damping rate of standard GAM (a), low frequency eigenmode (b), and ISW-like eigenmodes (c) as functions of q for different τ .

"Others" (from dust to …. and to runaway electrons)

Fulop: impurity transport in ITER seems to be OK -> neoclassical and anomalous (reactive drift wave model) impurity transport are of the same order; due to temperature screening neoclassical transport does not result in impurity accumulation in the core; anomalous transport causes inward pinch, but inward pinch of D/T is larger

Van Milligen: pulse propagation in probabilistic transport model involving transport enhancement at gradients exceeding critical one is considered

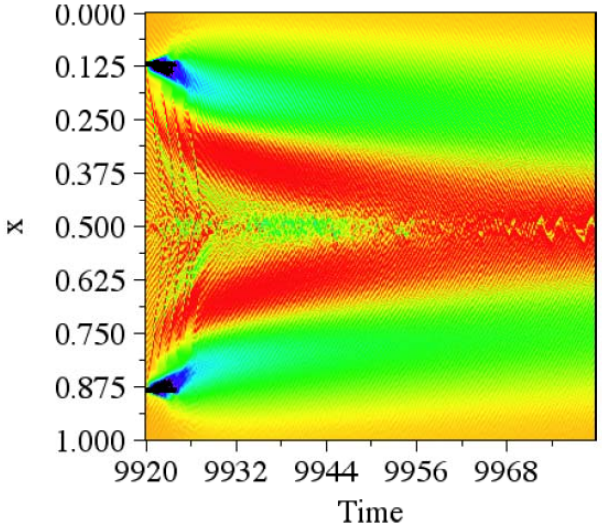

Krasheninnikov: conversion of re-deposited carbon in dust causes increase of radiation loss and eases divertor detachment

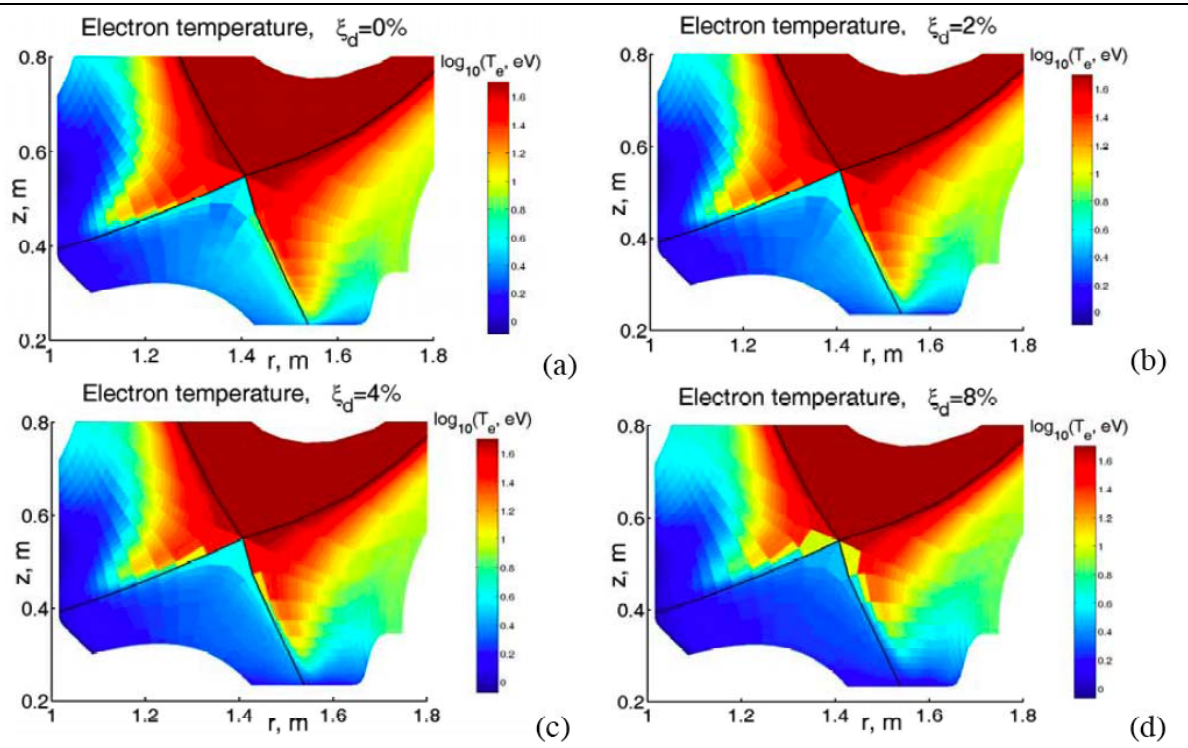

Gal: runaway electron generation by D killer pellet injection is analyzed for JET plasma; multiple injection of large pellets with velocities ~ 200 m/s is found to be a promising mitigation method; but, it is difficult to cool the plasma fast enough without causing runaway production

Surprises

No work on such long-standing and important issues as:

pedestal height in ITER

density limit

physics of first mm of the wall (redeposition, films, surface modification,

multi-material chemistry, hydrogen transport in wall material, etc.),

which is crucial for both ITER and DEMO!!!

Density limit cannot be expressed with a “standard” set of dimensional parameters: β, ν_*, ρ_*

Additional parameter can be:

atomic physics - $T_e=I$

$$N= \beta(T_e=I)/ \rho_*(T_e=I)$$

number of particles in Debyi sphere - N_D

$$N= \beta^{1/2} \nu_* N_D$$

Do we have right physics in our models???!!!